Vision Res. Vol. 33, No. 8, pp. 1089–1107, 1993
Printed in Great Britain.

0042-6989/93 $6.00 + 0.00

Inhomogeneity and Anisotropies for Motion Detection in the Monocular Visual Field of Human Observers

W. A. VAN DE GRIND,*† J. J. KOENDERINK,*‡ A. J. VAN DOORN,*‡ M. V. MILDERS,* H. VOERMAN*

Received 16 March 1992; in revised form 21 October 1992

Signal-to-noise-ratio (SNR) thresholds were measured for the detection of coherent motion in moving random pixel arrays of constant root-mean-square contrast (35%) and constant average luminance (48 cd/m^2) for 8 or 16 directions of motion at 25 positions in the visual field of the right eye. Five observers took part in this perimetric study of motion detection. The 24 eccentric positions were chosen on 8 equally spaced radial lines at the eccentricities 6, 24, and 48°, the 25th position was centred on the fovea. At these positions we analysed the threshold SNR-value as a function of motion direction α. A significant modulation of the threshold with α is called an anisotropy. Anisotropies were found for low to medium velocities at positions on and near the vertical meridian, where the thresholds proved to be highest for vertical motion directions (up or down). On the horizontal meridian no significant anisotropies were found. Also on the oblique radials anisotropies were found, especially at 225° (lower nasal quadrant of the visual field, upper temporal quadrant of the retina), but these were milder than those on the vertical meridian. The diameter of the stimulus is an important parameter and its influence was explored, albeit incompletely. Also inhomogeneities were found. This is defined as a consistent modulation of the threshold SNR-value with position A, the position along an equi-eccentricity circle (A-inhomogeneity), or with eccentricity E (E-inhomogeneity) or both. A simple acuity-scaling optimized for the nasal retina takes care of most of the E-inhomogeneity, but an A-inhomogeneity stays rather prominent. It too is characterized by higher thresholds near the vertical meridian than near the horizontal meridian. The findings suggest that iso-threshold curves are elliptical or egg-shaped with their long axis on the horizontal meridian and shifted somewhat out of naso-temporal symmetry towards the nasal half of the retinal field. As with the anisotropies the inhomogeneity grows in amplitude for decreasing velocity below medium velocity values of 1–2 pixels/frame, but in contradistinction to the anisotropies it is present and even increases in amplitude for increasing velocities above these medium values of 1–2 pixels/frame as well. The results are discussed in the light of other perimetric studies of motion detection and acuity, in the light of a model postulating the cooperation of groups of velocity-tuned bilocal motion detectors, and in the light of recent ideas on structure and function of primate cortical areas and processing streams.

Motion detection Motion anisotropies Inhomogeneities of the visual field Motion perimetry

INTRODUCTION

It is generally acknowledged that an adequate visual analysis of the optic flow field has a high survival value for animals and is a desirable goal for machine vision systems. At a mobile vantage point the optic flow field is usually inhomogeneous and anisotropic. For example, while walking in an open field the optic flow in the lower and upper visual field can be strikingly different. Moreover, foveofugal motion near the vertical retinal meridian in the upper retina might inform us on egomotion relative to the ground plane, whereas motion perpendicular to that meridian and near to it might be less interesting to control natural forward locomotion. To the extent that animals are "tuned" to their visual habitat they might capitalize on these and other facts. This would lead one to expect specialized regions in the visual field and/or the retina that are more sensitive to certain aspects of the flow at the expense of sensitivity to other aspects. If optic flow analysis is based on information provided by front-end motion detectors this entails the possibility of inhomogeneities and anisotropies of motion detection. This is the question we address in this paper: does the visual system of man show inhomogeneities and anisotropies of motion detection? The answer proves to be affirmative so one might

*Utrecht Biophysics Research Institute, The Netherlands.
†Department of Comparative Physiology, Utrecht University, Padualaan 8, 3584 CH Utrecht, The Netherlands.
‡Department of Medical and Physiological Physics, Buys Ballot Laboratory, Utrecht University Princetonplein 5, 3584 CC Utrecht, The Netherlands.

then ask whether the inhomogeneities and/or anisotropies can be related to special functions like analysing motion relative to the ground plane, or motion in the sky, keeping one's balance, changing course or moving body-parts (including the eyes). These more general questions regarding the possible role of anisotropies and inhomogeneities of motion perception are not addressed in this paper. The pattern of results proves to be rather complex in detail and certainly does not invite any facile interpretations. This is an empirically oriented paper, aiming to explore anisotropies and inhomogeneities in the monocular visual field as completely as possible. The strength lies in the data rather than the ideas. Several aspects of the findings might provide fertile ground for future speculations regarding the possible functional role (of anisotropies and inhomogeneities) and/or the underlying structure. These opportunities for speculation will be pointed out in the discussion.

Several previous reports indicate inhomogeneities and/or anisotropies of motion detection in humans. For example, the "optimal velocity" increases with retinal eccentricity (van de Grind, van Doorn & Koenderink, 1983), and there appears to be a difference between the perception of foveofugal and foveocentric motion (Ball & Sekuler, 1980; Georgeson & Harris, 1978; Mateeff & Hohnsbein, 1988; Mateeff, Yakimoff, Hohnsbein, Ehrenstein, Bohdanecky & Radil, 1991b; Mateeff, Bohdanecky, Hohnsbein, Ehrenstein & Yakimov, 1991a). On theoretical grounds foveofugal motion in the upper half of the retina near the vertical meridian, especially near the eccentricity of 45 deg, should be most informative with respect to ego-motion relative to the ground-plane of, say, a walking human (Koenderink, 1986). One might thus expect a higher sensitivity near that position for foveofugal motion than, for example, for a direction perpendicular to the vertical meridian, that is tangent to the equi-eccentricity circle of 45 deg. In a series of pilot experiments we found to our surprise just the opposite result! This result suggested that motion across the vertical meridian is easier to detect than motion along the vertical meridian, which we found *a priori* unlikely on anatomical grounds. Already this curious result seemed worthy of a further more detailed investigation. Moreover, a literature search showed that all perimetric explorations of motion detection so far were rather incomplete or failed to acknowledge the change of acuity with eccentricity or used only a class of targets (like spots or lines) that are nowadays regarded as unfortunate choices or did not measure anisotropies. Taken together this seemed to be sufficient reason for a perimetric study with the modern tool of moving random pixel arrays with a variable signal-to-noise ratio (van Doorn & Koenderink, 1982a, b).

In a recent paper Scobey and van Kan (1991) report perimetric results on displacement sensitivity and they report a lower threshold for tangential (to iso-eccentricity circles) as compared to radial displacements. This is similar to our results on movement detection (van de Grind, Koenderink, van Doorn, Milders & Voerman, 1990). However, the visual task of their subjects was to detect displacement, which is obviously different from the detection of coherent motion, notably the direction of movement, in random pixel arrays. For example, they report that the sensory experience was "that something changed in the visual field; probably the subject would not have been able to differentiate well between a luminance change or the displacement" (Scobey & van Kan, 1991, p. 108). In our case on the other hand the subjects had to set the threshold for the detection of the direction of coherent motion. Nevertheless, it is of interest to compare the results of the two studies in the Discussion. The paper by Scobey and van Kan (1991) also gives a useful review of the literature on asymmetries found in dendritic trees of retinal ganglion cells and on the recent literature describing a naso-temporal asymmetry in visual perception. Since we scaled all our stimuli according to the change of acuity with eccentricity along the nasal horizontal retinal meridian (van de Grind *et al.*, 1983) any inhomogeneities and anisotropies of acuity might show up in our results. It is known that acuity is neither completely homogeneous nor isotropic throughout the visual field (e.g. Fiorentini & Berardi, 1991), so we will have to relate our perimetric findings on motion detection to those on acuity.

METHODS

Choice of sampling positions, directions, eccentricities and of stimulus scaling

We used 8 positions spaced equally around equi-eccentricity circles and at each of the 8 positions 8 (in some cases 16) directions of motion were tested, as indicated for one eccentricity in Fig. 1. In the actual experiment we left the display at a fixed central position and changed the fixation point. The parameters A (angular position) and E (eccentricity), defined in Fig. 1,

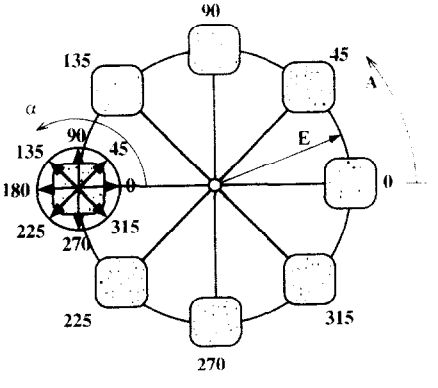

FIGURE 1. Definition of the position and direction variables of the experiment. Variable A is called the "position" of the stimulus and is given in degrees, α is called the "motion direction" and is also given in degrees, E is the eccentricity and is given in degrees of visual angle. In fact we did not reposition the monitor to change E or A, but the fixation point. The monitor could be rotated about an axis perpendicular to the centre of the screen to change α and it was mounted on rails to facilitate the changes of viewing distance that were necessary to scale the stimulus dimensions (pixel size and window diameter in degrees of visual angle) with eccentricity. The actual display aperture was circular. The rounded square in this figure was only used for artistic reasons.

specify the position of the stimulus in the monocular field of view of the observers. The parameter α specifies the motion direction of the moving random pixel array, as indicated in Fig. 1.

Since the peripheral field has a lower spatial resolution than the fovea a fair comparison of different eccentricities requires some form of scaling. We have previously shown that a scaling according to acuity leads to the simplest description of results obtained as a function of E along the horizontal meridian of the nasal retinal field of view (van de Grind *et al.*, 1983; van de Grind, Koenderink & van Doorn, 1986). If the ratio of the pixel diameter to visual acuity is constant (e.g. near 1) motion detection threshold signal-to-noise ratios (SNRs) are about equal in that case at all eccentricities for equal scaled stimulus velocities and scale stimulus sizes. Even though optimal eccentricity invariance requires a subject-dependent scaling, very good results were obtained for motion detection in the visual field of the nasal retina with an average pixel-size scaling according to

$$P(E) = P(0) \cdot (1 + E/E_h). \quad (1)$$

Here E_h is the eccentricity where the acuity equals half the foveal acuity value (E_h was found to be about 4°) and $P(E)$ is the pixel diameter used at eccentricity E when the pixel diameter used for foveal measurements is $P(0)$. Of course to obtain approximately equal thresholds at different eccentricities an additional requirement is that one uses about equal numbers of moving pixels. In the case of a fixed number of pixels moving within a display window of a fixed size one can implement the scaling of formula (1), as we did, by changing the viewing distance in such a way that formula (1) holds for the viewing window size in degrees of visual angle (replace pixel size P by window size W).

It was our original intention to explore the eccentricities 0, 3, 6, 12, 24, 48°, that is 41 positions, for five observers, the whole velocity range at each position for 16 directions of motion and all this for a range of stimulus sizes. Pilot experiments convinced us that this was not only far too time consuming, but also unnecessary. For relatively large stimulus sizes the field was reasonably homogeneous and isotropic and nothing of interest could be added to our previous results for the horizontal meridian of the nasal retina (van de Grind *et al.*, 1983). Inhomogeneities and anisotropies are masked at large stimulus sizes, because (1) thresholds are then near minimal virtually everywhere in the field (for appropriately scaled stimuli), and (2) the results are less "local" and thus smear out any local differences. At small stimulus sizes thresholds are high even for the optimal velocity (van de Grind *et al.*, 1983) so the velocity range that can be covered is rather small. Also, the steep increase of the threshold away from the optimum velocity for these small sizes (*op cit.*, Fig. 1) causes a high variance of the data unless one samples the velocity range near the optimum value very densely. Thus the interesting range of stimulus sizes is relatively narrow. To be able to test a wide range of velocities at every position, and to give the anisotropies and inhomogeneities a chance to express themselves by doing a reasonably "local" measurement, the stimulus size has to be on the order of 1–1.5 deg in diameter if referred via the scaling-relation to the fovea (the fovea, however, is reasonably isotropic for these or larger stimulus dimensions). Thus, the acuity-scaled equivalent of a fovea full of moving random pixels reveals the inhomogeneities and anisotropies discussed below.

The pilot experiments for our five subjects (JK, AD, WG, MM and HV) showed a high similarity of the results with qualitatively the same inhomogeneities and anisotropies. This led to the decision to sample the visual fields of JK, AD and WG at only one eccentricity ($E = 24°$) and one velocity (1 pixel/frame) but all 8 positions (45° apart) times 16 directions (22.5° apart). The visual fields of MM and HV were studied much more extensively at the eccentricities 0, 6, 24 and 48°, at all 8 positions for the non-zero eccentricities and for 8 motion directions at every position for a velocity range from 1 pixel shift per 8 frames (with a 10 msec frame-duration) to the high velocity cut-off in steps of a factor of 2. Each of these 1600 measurements for MM and HV consisted like the others of 16 values, the turning points of an up–down threshold setting method. Together with the pilot experiments (covering also some other eccentricities, such as 3 and 12°) this means that about 42,000 data points were gathered for each of our two main observers MM and HV and about 150,000 data points for all five observers taken together. This constitutes a substantial data base ensuring sufficient reliability and generalizibility of the overall pattern of results reported below. Because of the complete compatibility with the methods used in our previous studies at eccentricities from 0 to 48° along the nasal part of the horizontal meridian of the right eye of JK, AD and WG (van Doorn, Koenderink & van de Grind, 1984, 1985; van de Grind *et al.*, 1983, 1986; van de Grind, Koenderink & van Doorn, 1987, 1988, 1992; Koenderink, van Doorn & van de Grind, 1985) one can use the data from these previous studies as a supplement to the present perimetric results. Notably it was reported previously, that the threshold SNR-values are roughly independent of the direction of motion for positions on the horizontal meridian of the right eye (van Doorn *et al.*, 1985). Thus we found "isotropy" in the sense of the present paper for movement detection at these positions in the monocular visual field.

The stimulus and the SNR-method

The moving pattern consisted of (approximately) square random pixel arrays of 250 × 255 pixels shifted n pixels every mth frame at a frame-rate of 100 Hz, where the pixels that shifted out of the viewing window were deleted and new pixels were generated on the opposite side to enter the viewing window. To remove the cue of the square window in judging the directions of motion we covered the oscilloscope display by an opaque mat-black screen of 2 × 2 m with a circular aperture of 250 mm diameter centred on the display area. Since the

pixels were about 1 × 1 mm in size this means that the diameter of the aperture equals about 250 pixels (horizontally: 255 vertically). In all the stimulus therefore consisted of about 50,000 pixels. The oscilloscope could be rotated mechanically (360° continuously) to change the motion direction α. A light emitting diode was used as a fixation mark, except in foveal testing, when a black dot (size about 3 × 3 pixels) was pasted on the centre of the screen. The moving random pattern on the oscilloscope screen was degraded in a special way by noise arrays, consisting of 250 × 255 pixels that were newly generated every frame by a maximum length shift register. If the pattern pixels have luminance values $L - \Delta L_P$ ("black") and $L + \Delta L_P$ ("white") respectively, whereas the black and white noise pixels have the luminance values $L - \Delta L_N$ and $L + \Delta L_N$, the root-mean-square (r.m.s.) contrast of pattern and noise are $r_P^2 = (\Delta L_P/L)^2$, and $r_N^2 = (\Delta L_N/L)^2$, respectively. An electronic pixel by pixel addition of the noise and pattern arrays is performed in such a way, that the SNR $= r_P^2/r_N^2$ is determined by a subject-controlled push-button, while the total r.m.s. contrast $C = \sqrt{r_P^2 + r_N^2}$ is kept constant at 35%. [Readers who are unfamiliar with this type of contrast definition are referred to a didactic exposition by Moulden, Kingdom and Gatley (1990).] Our method could be called a "luminance"-SNR method to prevent confusion with "spatial"-SNR methods in which pixel-correlations between successive frames are manipulated not by changing their luminance correspondence but by changing their positional correspondence or by randomly flipping the sign of a given percentage of pixels between frames, etc. For a comparison of some of these methods and their results see Fredericksen, Verstraten and van de Grind (1993). In our hardware stimulus generator the prevailing SNR value, as set by the subject, set a readout pointer in an electronic look-up table where the corresponding ΔL_N values and ΔL_P values are stored. The sign of each is determined by the corresponding bit values of the pattern pixels and noise pixels (zero's map onto minus and ones onto plus signs) as generated by maximum length shift registers of 32 bits ($2^{32} - 1$ states). The z-axis signal to the oscilloscope thus shows the voltage levels corresponding to the sum of the average luminance and the increment luminance levels $-\Delta L_P - \Delta L_N$ (=0,0), $-\Delta L_P + \Delta L_N$ (=0,1), $+\Delta L_P - \Delta L_N$ (=1,0), and $+\Delta L_P + \Delta L_N$ (=1,1). The SNR-value can be adjusted by the subject in 0.2 dB steps over a 6 log unit range (from 10^{-5} to 400). The resulting random-pixel cinematograms are displayed on a Hewlett–Packard model 1317A oscilloscope with a P4 phosphor. The average luminance on the screen was kept constant at 48 cd/m^2, the room was dark. The size of the display in degrees was adjusted by changing the viewing distance appropriately.

The cut-off frequency of the white spatial frequency spectrum of the random-pixel arrays is thus scaled to lower values as well with increasing E, since it is inversely proportional to the pixel size. The temporal properties of the target arrays are mainly determined by the velocity control, which enforces a jump of n pixels every mth frame. Thus receptive fields with a more sluggish reaction will favour a higher m and fast neurons will favour a lower m, the single array exposure duration being $10\,m$ msec ($=m$ frames). The noise has a temporal cut-off frequency of 100 Hz in all cases, which means that neurons with a wider temporal pass-band will pick up more noise power. Under photopic circumstances this is not expected to play an important role since all receptive fields are expected to be reasonably fast with a more or less comparable temporal pass-band. During dark adaptation on the other hand more and more of the temporal noise is averaged. Under those circumstances the present equipment does not allow the use of a signal to noise measurement and different methods have to be used. A substantial improvement of the stimulus hardware and software to allow better control of the spatio-temporal spectrum of both the target arrays and the noise arrays has been accomplished by Fredericksen *et al.* (1993). This improved approach also allows a comparison or even mixture of the luminance SNR and spatial SNR methods and has validated the major results (only those were checked) obtained with the present set-up.

Subjects and task

The subjects AD, WG, JK are very experienced in many types of psychophysical visual experiments and had more than 9 yr of experience with the task of setting the SNR threshold for the detection of coherent movement in this type of set-up. MM and HV were new to the task but they performed extensive series of training and pilot experiments before embarking on the present perimetric study. The former three subjects are middle-aged, the latter two around 24 yr of age. All had normal or corrected to normal vision. No visual defects or abnormalities were found for our subjects with the usual techniques of testing vision, including informal perimetric tests. The right eye was used in all cases and the left eye was covered with an eye-patch during the experiments. The task of the subject was to lower the SNR-value until the percept of coherent movement (with a clear motion direction) gave way to the percept of "snow" without overall drift, then to increase the SNR-setting again until coherent motion was just perceived, then lower the SNR-value again, etc. After 16 turning points the settings were read out (copied by hand from a memory display). Although the stimulus was on all the time, the subjects were instructed to look away from the screen during the pauses. These pauses lasted 10 or more sec at a time, while the turning point data (all 16 values) were recorded and the stimulus parameters were changed by the experiment leader. The first two of the 16 turning point values were discarded during the analysis and from the other 14 settings we calculated the average, standard deviation, and several other statistical parameters (e.g. to check for drifts and hystereses phenomena). The average of these 14 turning points is called the thrshold SNR value, S. It is the main quantifier of the performance. It has been our experience that even completely inexperienced subjects can easily set the SNR-threshold

and that they do so reliably and reproducibly. It is an easy task. The standard deviation of the 14 settings is usually on the order of 1–3 symbol diameters in the graphs of this paper. This should not be confused with repeatability statistics. If a certain threshold measurement is repeated on different days the variance of the different outcomes depends upon the average threshold level. At SNR-values below 1 the variance is always $<20\%$ of the mean (the smaller the threshold the smaller this relative variance), but for higher threshold SNR-values the variance increases strongly. This is understandable from the fact that the SNR-method strongly amplifies the difference between "just seen" (say an SNR-value of 50) and not seen (SNR-value infinite).

Bischof and Di Lollo (1990) have recently argued against the use of staircase methods for bandpass-filtered moving random pixel arrays and in favour of forced-choice procedures estimating the percentage of correct choices between two randomly presented motion directions (right–left). Their argument was based on the fact that the percentage of correct responses was a non-monotonic function of displacement distance in a two-frame presentation paradigm. However, their results for non-filtered stimuli, as we have used, are monotonic and would thus allow a staircase procedure. The comparison may not be unrestrictedly valid, however. In our set-up we have a more nearly natural type of motion stimulus, with 100 frames per sec and not compromised by the limitation of only two frames and wrap-around pixels. In our experience and for our type of stimuli forced-choice experiments give exactly the same results as staircase procedures, it only takes much longer to gather the data. With the amount of data needed for the present project a forced-choice design would have taken years of data collection. Fortunately the results of Bischof and Di Lollo (1990, their Fig. 7h) independently support the validity of our choice, at least to the extent that the detection tasks are comparable.

RESULTS

Preparatory experiments

In this paper we define an anisotropy as a (significant) modulation of the threshold SNR-value as a function of α, the movement direction of random pixel arrays displayed within a round aperture. This should not be confused with another anisotropy phenomenon reported previously for motion detection within a rectangular window. In that situation detection thresholds depend upon the direction of motion (Chang & Julesz, 1983; van Doorn & Koenderink, 1984). Assuming that the cooperative behaviour of bilocal motion detectors (van Doorn *et al.*, 1984, 1985) underlies movement vision one expects the anisotropic form of the elementary detectors to play a role in spatial summation. A bilocal motion detector like the Reichardt correlator mechanism (Reichardt, 1961) or one of its many variants (e.g. van Doorn & Koenderink, 1983; van Santen & Sperling, 1984, 1985), has two not completely overlapping receptive fields, the outputs of which are combined via a delayed multiplication. Thus, the detector is longer in the direction of motion to which it is tuned than in other directions. The limiting size of a rectangular window (a "strip") filled with moving pixel arrays will therefore be larger if the short side is parallel to the motion direction than if the long side is turned in the direction of motion. This expectation was borne out in the sense that the threshold (size or SNR value) measured with relatively narrow strips filled with moving pixels was lower for movement in the direction parallel to the long side than in the direction perpendicular to the long side (Chang & Julesz, 1983; van Doorn & Koenderink, 1984; van de Grind *et al.*, 1986). For a round aperture this effect should play no role, and if there are approximately equal numbers of detectors for each motion direction one would expect isotropy, that is a flat graph if S (the threshold SNR-value) is plotted against α. This is the result found for the position $A = 0°$ at $E = 24°$ for the three observers in Fig. 2.

Among other things Fig. 2 illustrates that one can find anisotropies for one observer for stimulus parameters for which other observers appear to give isotropic results. For example, observer JK (triangles in Fig. 2) does not show much of a threshold modulation with α at any of the eight positions at this eccentricity of 24° and at this medium velocity of $V = 1$ pixel/frame for the chosen stimulus diameter of 8°. The other two observers show strong anisotropies, especially at the positions on the vertical meridian ($A = 90$ and 270°), where no coherent motion was detected at all (infinite threshold-value S) in half of the cases of centrifugal or centripetal motion ($\alpha = 90$ or 270°, the vertical directions of motion). In order to be able to plot these curves with a computer we chose a large number (10^6) to represent infinity, thus the lines towards infinity do not have an infinite slope in Fig. 2.

We did not yet know what to expect when we carried out this initial experiment with the three senior authors as subjects, except that we knew the positions along the nasal retinal meridian ($A = 0°$) to give isotropic results (van Doorn *et al.*, 1985). After plotting Fig. 2 we wondered why no anisotropies were found for JK and we therefore explored the influence of the stimulus size on his results at positions on the vertical meridian. It proved that a slight decrease of the stimulus size (10–20%) made his results similar to those shown for the other two observers in Fig. 2. Conversely, a modest increase of the stimulus diameter strongly diminished or even completely eliminated the anisotropies for the other two observers (AD and WG). If one wants to bring out the anisotropies at this one velocity it is apparently necessary to choose an optimal stimulus diameter for each observer separately. At the eccentricity of 24° and for our type of stimulus these optimal sizes ranged between 6 and 10° in diameter (five observers, see also Fig. 3). This is the eccentricity-scaled equivalent of 1–1.5° in the fovea [formula (1), with $E_h = 4°$]. In interpreting these and the later results the reader should keep two things in mind. In the first place we wanted to measure motion detection properties as "locally" as

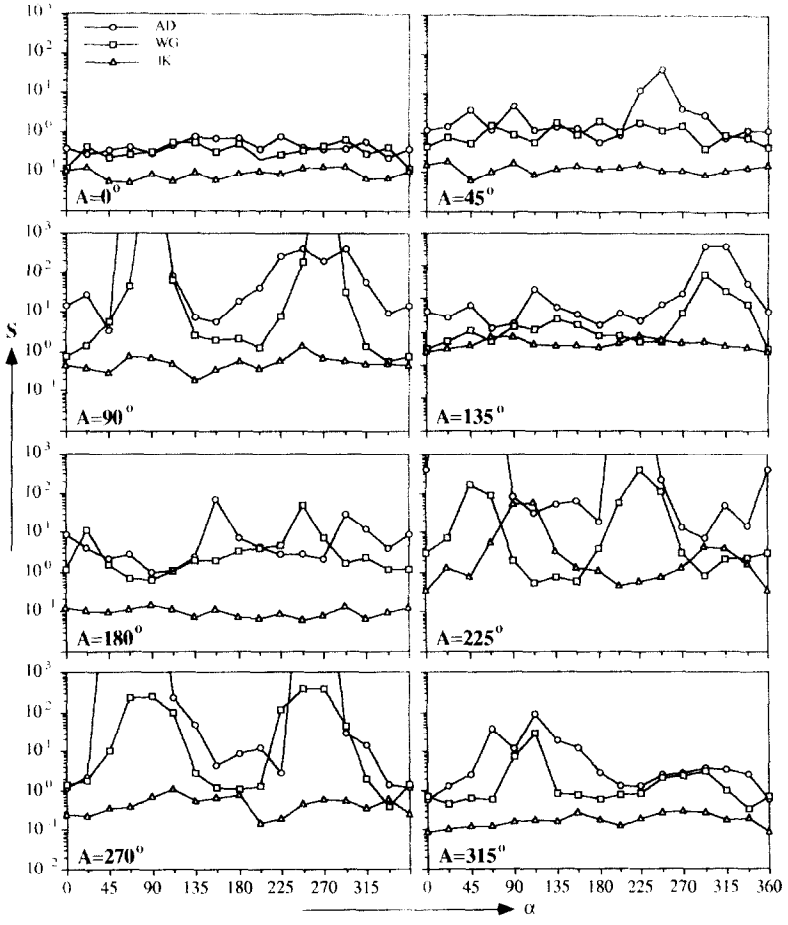

FIGURE 2. Threshold SNR values, S, plotted as a function of the motion direction α for three observers (AD, WG, JK). The scaled velocity was $V = 1$ pixel/frame, the eccentricity 24′ and the position A as indicated in the eight panels. Motion direction was sampled at intervals of 22.5°, leading to 16 sample points per graph. Infinite threshold values (no coherent motion seen, even without noise) are represented by a large but finite number (1,000,000) to facilitate automatic plotting. This leads to finite (but high) rather than infinite slopes (vertical lines) at places where the neighbouring point represents an infinite threshold. The inset in the panel for $A = 0°$ shows what symbols are used for each of the three observers. Strong anisotropies can be seen for the observers AD and WG at positions along the vertical meridian ($A = 90$ and 270°) and near to it (e.g. $A = 225°$). The results at $A = 0°$ typify isotropy.

possible, which means that one has to choose small stimulus sizes and this automatically leads to measurements in a relatively low motion sensitivity range. The base line SNR values are therefore already 10 or 100 times higher than for easily detected sufficiently large stimuli [which have SNR threshold values from 0.04 to 0.1: van de Grind *et al.* (1983)]. In the second place the subjectively small range from "hard-to-detect-but-still-visible" to "not seen" is mapped onto a huge SNR value range from, say, 10 or 100 to infinity. Therefore, slight decreases of the size can, as was discussed for Fig. 2, lead to an SNR threshold that shoots upwards in the graph. This is a strong point of the method (sensitivity). One can also conclude from Fig. 2 that a simpler method to quantify the anisotropies and inhomogeneities would be to measure the threshold *size* for the detection of coherent motion in normal random-dot patterns, that is without the luminance SNR method. Our method has the added feature that it also allows quantification of suprathreshold sensitivities to motion, and we thus preferred it. Another question that resulted from inspection of Fig. 2 was whether the highest threshold differences are found between the head-centric horizontal–vertical directions or between the radial–tangential directions. The radial directions are foveofugal (to be called centrifugal) or foveocentric (to be called centripetal), the tangential directions are the clockwise or counterclockwise directions along the tangents to equi-eccentricity circles. Results for the observers AD and WG at $A = 135°$ and 225° in Fig. 2 suggest the latter, that is radial–tangential, option ($\alpha = A$ and $\alpha = A + 180°$ are the centrifugal and centripetal directions, respectively, whereas $\alpha = A + 90°$ and $\alpha = A + 270°$ are the counterclockwise and clockwise tangential directions, respectively). At $A = 225°$ there is even an indication of a threshold modulation with α for JK, but it does not fit the centrifugal–centripetal idea. We will return to this question of radial–tangential vs horizontal–vertical anisotropies in the analysis of results for the two junior observers MM and HV.

Figure 2 conveys one more surprising message. If one inspects the average level of the graphs in each of the panels it becomes clear that the overall threshold level changes with A. This is what we call an inhomogeneity. The results also indicate that this inhomogeneity is independent of the anisotropies, since it occurs for JK as

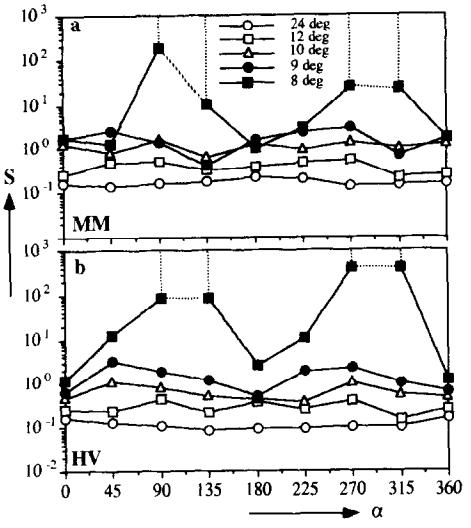

FIGURE 3. SNR threshold values, S, as a function of movement direction α for the subjects MM (A) and HV (B), measured at 24° eccentricity, position $A = 270°$ and one velocity, namely $V = 2$ pixels/frame. In other words the velocity was double the unit velocity given in Table 1 at 24° for each of the subjects. Strong increases of threshold can be seen at motion directions near 90 and 270° for the smaller stimulus sizes. With large stimuli, the thresholds are low for all directions of motion and no anisotropies can be discerned.

well as for the other two observers. The characteristic properties of this inhomogeneity appear to be that the threshold is highest along the vertical meridian ($A = 90$ and 270°), lowest along the horizontal meridian ($A = 0$ and 180°), and intermediate at the four oblique positions. Furthermore, the thresholds in the nasal half of the retina are lower than at comparable positions in the temporal half of the retina (cf. 135 to 45°, 180 to 0°, and 225 to 315°). This naso–temporal asymmetry might correlate with a similar asymmetry in ganglion cell counts (see Discussion).

On the basis of these initial explorations we decided to do a somewhat more complete perimetry, namely at the fovea and three eccentricities (6, 24 and 48°), for the full range of velocities, and along the same 8 radials. To make this feasible we had to restrict the number of motion directions to 8, rather than the 16 used in Fig. 2. Furthermore, we decided to limit the full perimetry to two subjects (the junior authors MM and HV), and, where and if necessary, to check characteristic results for the other three observers. As remarked above one first has to choose a stimulus diameter for each subject that is likely to bring out the anisotropies and inhomogeneities with sufficient clarity. For a large stimulus width (in degrees of visual angle) S values are very low in all movement directions (α), so anisotropies are virtually indiscernible. If one gradually decreases the stimulus size thresholds increase, but after a certain point they increase more strongly for certain movement directions than for others: Fig. 3. If one decreases the stimulus size too much all thresholds become very high or infinite and it is consequently impossible again to visualize any anisotropies. Thus there is a optimal stimulus size to quantify anisotropies. For the two main subjects of the rest of this study, MM and HV, we chose the stimulus width values of 9 and 10° respectively at the eccentricity of 24°. This was based on findings such as those of Fig. 3 for $E = 24°$, $A = 270°$, and $V = 2$ pixels/frame. The choice of velocity in the experiment leading to Fig. 3 was based on a more extensive (but less formal) pilot study, which showed that anisotropies disappear at higher velocities and increase in strength at lower velocities, whereas inhomogeneities increase both for higher and for lower (than medium) velocities. Velocities like $V = 1$ or $V = 2$ pixels/frame form a convenient compromise, where both anisotropies and inhomogeneities are just discernible at the optimal choice of the stimulus size, without unduly masking each other.

Figure 3 shows that both observers had strong anisotropies at a stimulus diameter of 8°. Since we wanted a just indiscernible modulation at this medium velocity (otherwise virtually all threshold values at the lower velocities would be infinite, except at $A = 0$ and 180°), we chose diameters $> 8°$ for both observers. Specifically we chose 9° for MM and 10° for HV. One could admittedly also have chosen equal diameter values for the two observers or somewhat larger values (e.g. 12°), but on the basis of the pilot studies we don't think such fine-tuning is very important. The characteristic pattern of anisotropies and inhomogeneities can be discerned for somewhat larger or smaller diameter values as well, provided the full range of velocities is explored. For smaller diameters anisotropies continue up to higher velocities and inhomogeneities are more extreme in amplitude; for larger diameters the modulations with A are more shallow and the anisotropies only show up at the lowest velocities. After having chosen the "optimal" stimulus diameter values for the two observers we used eccentricity-scaling formula (1) to calculate the "corresponding" stimulus widths at the other eccentricities. These values and the corresponding viewing distances, pixel sizes and unit-velocities (for $n = m = 1$, that is 1 pixel shift every frame) are given in Table 1.

Before presenting the more detailed findings it is useful to give an impression of the general pattern of results. Figure 4 gives such an overview for two velocities near and just below the middle of the scaled velocity range: one pixel shift between consecutive frames for observer

TABLE 1. Stimulus parameters to the two main subjects at the eccentricities 0, 6, 24 and 48°

Subject	E (deg)	W (deg)	p (min arc)	V (deg/sec)	L (mm)
MM	0	1.29	0.3	0.5	10,037
	6	3.22	0.76	1.27	4027
	24	9.00	2.12	3.53	1435
	48	16.77	3.95	6.58	766
HV	0	1.43	0.34	0.56	9054
	6	3.57	0.84	1.40	3625
	24	10.00	2.35	3.95	1291
	48	18.59	4.37	7.28	690

W is the width of the square stimulus in deg of visual angle, p is the pixel size in min of arc, V is the velocity at a shift speed of the pixel shift between consecutive frames at the frame frequency of 100 Hz. The viewing distance L is given in mm and it of course follows directly from the fixed screen size and the choice of W.

MM in (A), and 0.5 pixels/frame for observer HV in (B). The irregular octagons represent the threshold SNR values, S, plotted radially along the directions of motion on a log scale (inset) starting at $S = 0.1$ (the origin, indicated by a dot in the octagons). In other words, the vectors pointing to the corners of the octagons indicate the motion direction and have a length indicating logarithmically how much S exceeds the value 0.1. Infinite threshold values (no coherent motion seen even without noise) are set equal to the relatively large value of 400 to get closed octagons in this "symbolic" representation of results. Note also that the radial distance between the equi-eccentricity circles is not proportional to the eccentricity differences, but constant. This symbolic representation is well-suited to give an intuitive impression of the inhomogeneities and anisotropies to be quantified below.

Figure 4 shows that the lowest thresholds (for our scaling regime!) are to be found at an eccentricity of 24′, whereas the thresholds at $E = 6$ and 48′ are mutually comparable and somewhat higher. If we compare thresholds at the 8 positions (A values) of any one eccentricity we see that the thresholds are higher the closer one gets to the vertical meridian. The differences between the horizontal and vertical meridian are especially striking for the eccentricities of 24 and 48′. If we take the area of the octagons as a rough indication of the threshold at a given position (A,E) it is clear that the differences between mirror positions on the nasal retina ($A = 0, 45, 315$°) and the temporal retina (A = 135, 180, 225°, respectively) is small for the eccentricities 6 and 24′. At an eccentricity of 48′ on the other hand there is a clear asymmetry relative to the vertical meridian since the thresholds are much smaller in the visual field of the nasal retina than in the field of the temporal retina. Especially the difference between $A = 0$ and 180° is striking at $E = 48$′. Next let us compare results along the radii in Fig. 4. In the field of the nasal retina (right half of Fig. 4) thresholds are similar for all eccentricities along any radius (A = constant). This shows that our scaling of stimuli equates thresholds satisfactorily for the nasal retina. Not unexpectedly, this scaling proves to be less satisfactory for the temporal retina, for which it was not optimized. In that hemifield the threshold has a clear minimum near 24′ eccentricity, however, and such a non-monotonic change with E suggests a radially directed inhomogeneity rather than sub-optimal scaling parameters.

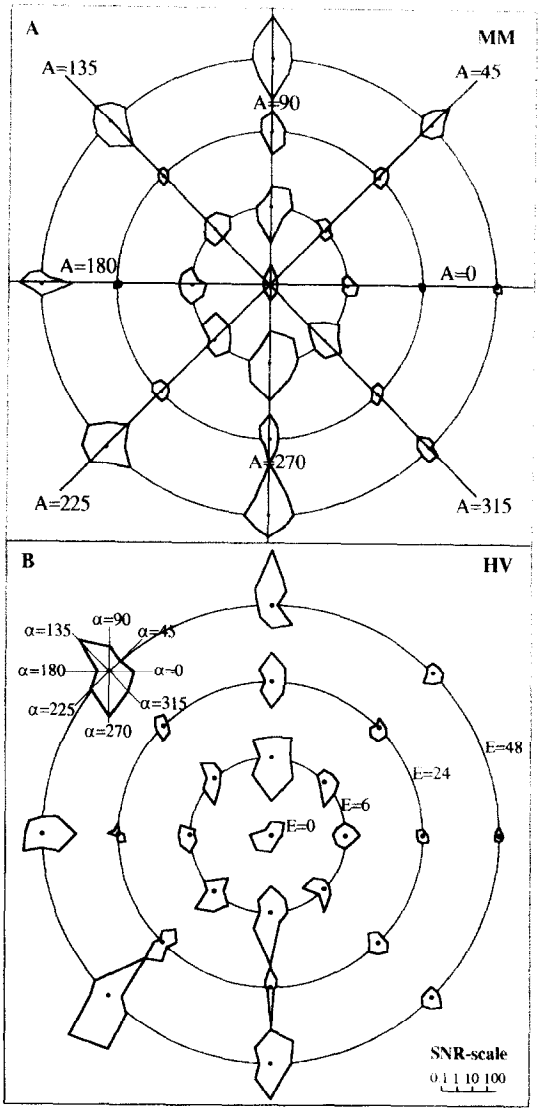

FIGURE 4. Threshold octagons as measured at all eccentricities and all positions used in the main experiment, but for only one velocity in each half of the figure, viz. 1 pixel per frame (unit velocity) in (A) (observer MM) and 0.5 pixel/frame in (B) (observer HV). A threshold octagon is obtained by plotting a vector in each of the eight directions of motion with a length proportional to the logarithm of the threshold SNR value, S, for that direction, and by connecting the vector end points. The common origin for the vectors is the position in the visual field of the measurement and the origin is assumed to represent S values of 0.1 (since zero cannot be represented on a log scale). The inset in the lower right hand corner of (B) shows the S-scale used in plotting the octagons. Infinite SNR threshold values were plotted as a value of 400 in order to keep the octagons closed.

With the help of Fig. 4 we can also clarify once again what we mean with "inhomogeneity" and "anisotropy", respectively. Inhomogeneity refers to the fact that the area of the threshold octagons depends on A and/or E. In fact we will only discuss the inhomogeneity found for constant E and variable A, the inhomogeneity along the circumference of an equi-eccentricity circle, in more detail. If the differences are relatively small in part of the visual field, as for example in a sector of the visual field of the nasal retina, that part of the visual field is "homogeneous", given our scaling regime [simple E-scaling, formula (1)]. Of course one can improve the apparent homogeneity of other regions by increasing the complexity of the scaling regime, for example by making the scaling factor a function of both E and A. We will return to this point and the problem of defining "homogeneity-after-scaling" in the Discussion. Anisotropy refers to the form of any one octagon of Fig. 4. If an octagon deviates significantly from a regular octagon, the sensitivity to coherent motion depends on the motion direction at that specific position of the visual field, which we call anisotropy.

Inhomogeneity

So far we have only illustrated results obtained at a few scaled velocity values, namely 0.5, 1 or

2 pixels/frame (Figs 2–4). It is known from previous work that S depends on velocity and it is not *a priori* likely (especially in view of the mentioned results of the pilot experiments) that the inhomogeneities and anisotropies of Figs 2–4 are velocity-independent. Let us first average out the influence of anisotropies to get an impression of the influence of velocity on inhomogeneities. To this end we average thresholds at any position (A and E constant) for all eight motion directions. The results are plotted in Fig. 5, which gives the average (across all directions α) of S plotted as a function of the normalized velocity (in pixels shift between consecutive frames) for each A value separately, and with E as a parameter. Data on observer MM are presented in Fig. 5(A) (upper two rows), those on HV in Fig. 5(B) (lower two rows). The panels are ordered anti-clockwise in accordance with the convention of Fig. 1 for parameter A. In this figure a vertical line denotes that the next higher or next lower velocity had an infinite threshold. No such lines are drawn if the next higher or next lower velocities were more measured.

Looking at the average vertical position of the graphs one can see in Fig. 5 that the lowest thresholds are found at $A = 0°$ for both subjects and all eccentricities. In general the highest threshold values are found near the vertical meridian, especially at $A = 90°$ (lower retina) but also near $A = 270°$ (upper retina). The width of these estimated velocity-tuning functions indicates the range of velocities that can be seen and it is clearly at a maximum for $A = 0°$, at all eccentricities.

It is remarkable that the optimal velocity is always near one or two eccentricity scaled pixels per time unit (of 10 msec) despite the large changes of threshold values with A. Thus scaling according to formula (1) indeed simplifies the comparison across A and E values. Since the velocity-range with finite SNR values is smaller near the vertical than near the horizontal meridian, the inhomogeneity is most pronounced for velocities near the low and the high end of the velocity range. For example, at normalized velocity values of $\frac{1}{8}$ and 8 both observers of Fig. 5 can detect coherent motion at $A = 0°$ for all eccentricities, whereas that is not the case at $A = 90°$. There subject MM only has a finite threshold at the high velocity end for $E = 24°$ [open squares in Fig. 5(A); the open circles are data for $E = 0°$ and they are repeated in all panels for the sake of reference]. For subject HV the threshold at $E = 48°$ is about 0.3 at $A = 0°$ and about 200 at $A = 90°$. For both subjects all

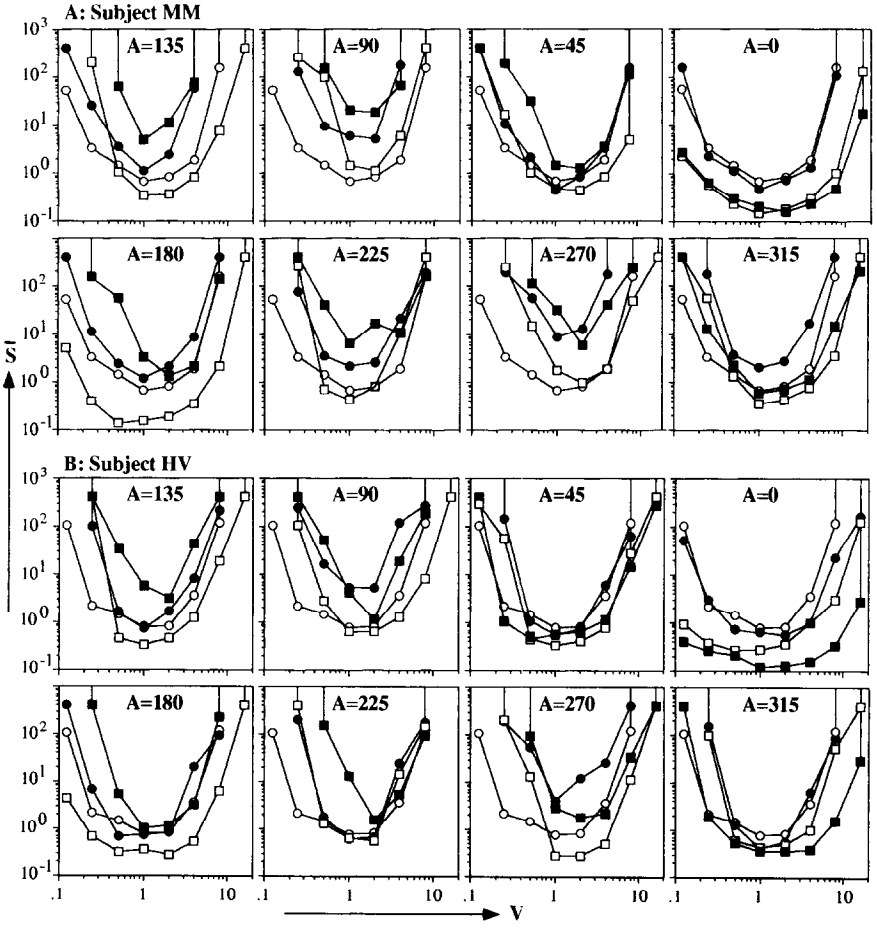

FIGURE 5. The 16 panels present direction-averaged threshold SNR values, S, as a function of scaled velocity V (pixels/frame), with the eccentricity E as a parameter. Each panel represents a different position A as indicated. The ordering of the panels conforms to the convention for A values given in Fig. 1. The results for observer MM are given in (A) (upper two rows), those for HV in (B) (lower two rows). To get an impression of the inhomogeneity of the visual field for motion detection SNR threshold values were averaged across the eight directions of motion for each position/eccentricity. Open circles, $E = 0°$ (identical in all panels for each observer); solid circles, $E = 6°$; open squares, $E = 24°$; solid squares, $E = 48°$.

thresholds at the lowest velocity ($\frac{1}{8}$) are finite at $A = 0$ and infinite at $A = 90$ and 270 .

To get a more global view of the inhomogeneity along equi-eccentricity circles one can average across the eccentricities 6, 24 and 48 . Inhomogeneities that are roughly eccentricity-independent will survive such an averaging, whereas eccentricity-specific inhomogeneities will be de-emphasized. The results for one observer (MM) are given in Fig. 6(A), where we have only plotted the data for the horizontal and vertical meridians in order to prevent cluttering of the figure. It is clear that the velocity range contracts and that thresholds increase strongly when going from positions on the horizontal meridian to positions on the vertical meridian. The lowest threshold values are found along the horizontal meridian on the nasal retina ($A = 0$), the next level of threshold-values is found on the temporal retina along the horizontal meridian, and the upper and lower fields compete for the highest threshold values along the vertical meridian. The full set of data-points of which Fig. 6(A) presents a subset can better be given in the format of Fig. 6(B), the transposed form of Fig. 6(A). In Fig. 6(B) the average SNR threshold values (averaged across motion directions and across non-zero eccentricities) are plotted against A, with velocity as a parameter. The symbols are chosen in such a way that the closed and open versions of each form represent velocities equally far above, respectively below, the optimal velocities of 1 or 2 pixels/frame. Thus it can be seen quite clearly that the inhomogeneity is strongest for the lowest and highest velocities ($\frac{1}{4}$ and 8 pixels/frame respectively), medium strong for the intermediate velocities (0.5 and 4 pixels/frame respectively) and least pronounced, although still substantial, for the optimal velocities (1 and 2 pixels/frame).

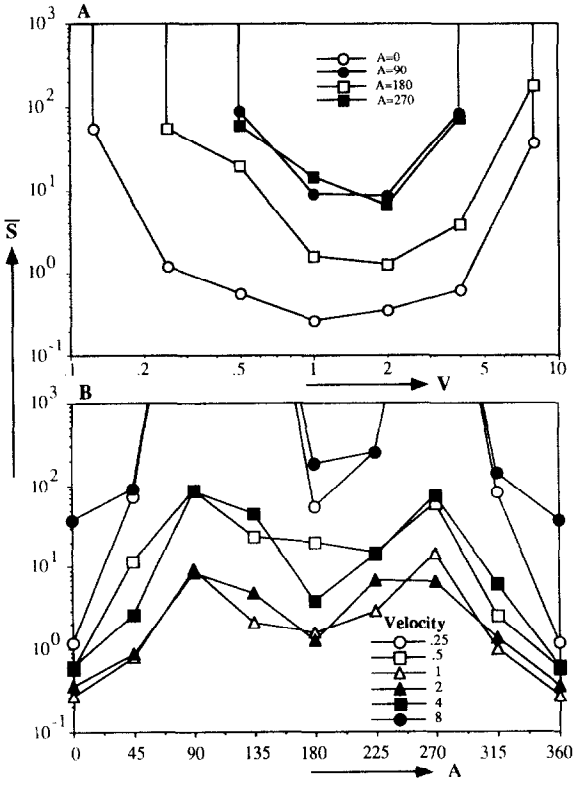

FIGURE 6. Summary of the main findings of Fig. 5 obtained by averaging the threshold values at each combination of the parameters A and V for the three eccentricities 6, 24 and 48 . Only the results for observer MM are presented, those for HV were highly similar. In (A) this averaged threshold is plotted as a function of the scaled velocity V for each of the four directions along the horizontal and vertical meridians. Data for the four intermediate positions are not included in (A) to prevent cluttering of the figure, but they can be found in (B), where the averaged threshold is plotted against (A) with scaled velocity as a parameter. (B) Is thus the transposed version of (A). The choice of symbols in (B) facilitates the interpretation. Open symbols are an optimal velocity (triangle) and lower velocities, solid symbols are an optimal velocity (triangle) and higher velocities. The same symbol-form denotes equal distance from the optimal velocity to the lower (open symbols) or higher (solid symbols) velocity side.

The results for the other observers are highly similar if plotted in this form and Fig. 6 conveniently captures the main trends in the inhomogeneities. Nevertheless we cannot rest our case here, because the anisotropies illustrated, e.g. in Fig. 4 might interact with the inhomogeneities or even be a major cause of the above findings of a change of the average threshold with A. To disentangle anisotropies and inhomogeneities we plotted SNR thresholds as a function of A [the format of Fig. 6(B)] for all combinations of motion directions (8 directions), velocities (8 velocities) and eccentricities (6, 24 and 48) separately and for both main observers (MM and HV). It is impossible here to reproduce these 384 graphs. Fortunately the results for the two observers are similar and the influence of eccentricity is negligible compared to that of A. Thus it is possible to average across eccentricities and to concentrate on one observer. This leads to the 64 graphs presented in the six panels of Fig. 7.

The general pattern of the results is simple: usually one finds maximum thresholds at the vertical meridian ($A = 90$ or 270) and minimum thresholds for the horizontal meridian ($A = 0$ or 180), whereas the threshold values for the other positions fall somewhere in between these extremes, and this holds for each direction of motion (parameter α). Of course the amplitude of the threshold change with A depends upon the direction of motion, and because vertical directions of motion ($\alpha = 90$ or 270) prove to give the highest thresholds (see the further quantification of anisotropies below) the anisotropy and inhomogeneity can add up when both A and α are near 90 or 270 . Nevertheless, the overall modulation of the curves in Fig. 7 is surprisingly similar for all values of α, showing (in line with the above findings for JK, reported in Fig. 2) that the anisotropy does not cause the inhomogeneity. One might, however, object that we have only plotted results in Fig. 7 for constant motion directions in a horizontal–vertical coordinate system (α = constant for all A in each individual graph of S as a function of A). What about possible radial–tangential anisotropies? Could they explain part of the inhomogeneity? To study this question we plotted the same threshold SNR values against A again, but now sorted together for centrifugal ($\alpha = A$), centripetal ($\alpha = A + 180$), clockwise tangential ($\alpha = A + 270$), and counter-clockwise tangential ($\alpha = A + 90$) directions of motion: Fig. 8.

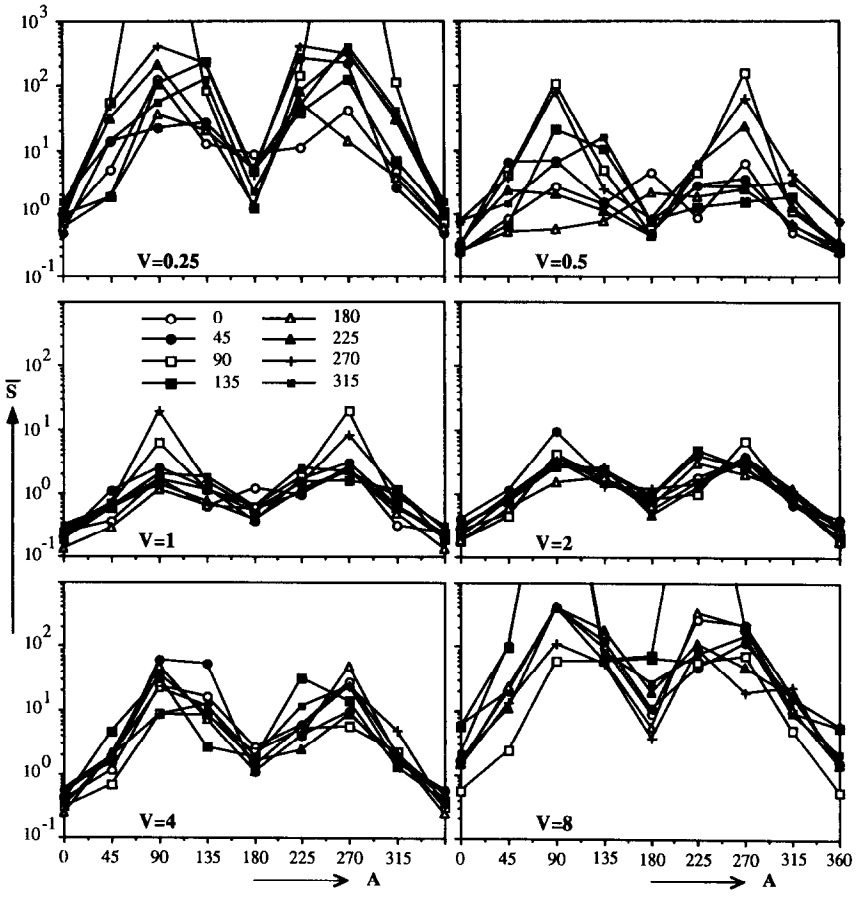

FIGURE 7. Average threshold SNR values, S, as a function of the position parameter A, with the direction of motion, α, as a parameter. Each panel presents data for a different scaled velocity value, as indicated. Observer MM. The data points represent values averaged across the eccentricities 6, 24 and 48°. The different symbols refer to different directions of motion as indicated in the inset in the panel for $V = 1$ pixel/frame.

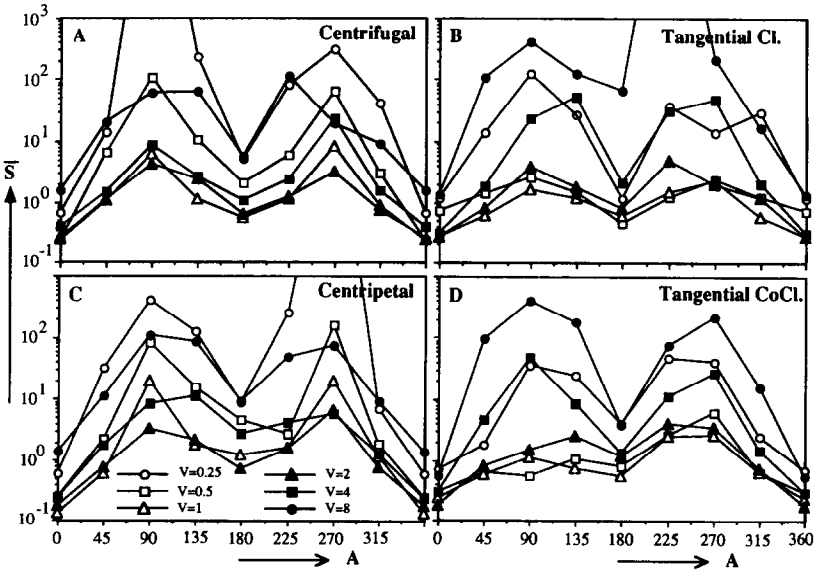

FIGURE 8. The format of this figure is similar to that of Fig. 7, except that the scaled velocity is now a parameter of the graphs (rather than the direction of motion as in the previous figure). Observer MM. Average S values are now sorted per panel according to the value pair (α, A), in such a way that each panel represents only data for one of the four main directions of a radial-tangential coordinate system. (A) Results for foveofugal, (C) for foveopetal motion, the other two panels for clockwise and counterclockwise motion along the tangent to equi-eccentricity circles. The threshold change with position A which we call an inhomogeneity is found in all four cases, as it was for the eight motion directions of Fig. 7, which were oriented in a vertical–horizontal coordinate system. The inhomogeneity is found for all motion directions and is strongest for low and high velocities.

Figure 8 again indicates that the overall pattern of the inhomogeneity is independent of the direction of motion (radial vs tangential), and that the amplitude of the inhomogeneity depends upon velocity. It is smallest for medium velocities (1 or 2 pixels/frame) and largest for high and low velocities. Together Figs 7 and 8 provide the evidence that the simple summary of Fig. 6 is indeed a valid description of the main aspects of inhomogeneity of the retina for the detection of coherent motion in targets of limited size. Anisotropies do not appear to interfere with or cause this pattern of findings. The latter conclusion is further substantiated below, where we will show that anisotropies are only present at lower than medium velocities, whereas the above results show that the inhomogeneity also shows up at higher than medium velocities.

In summary, for any eccentricity and motion direction, thresholds for the detection of coherent movement in our eccentricity-scaled stimuli of restricted size are smallest near the horizontal meridian and highest near the vertical meridian. The amplitude of the inhomogeneity (modulation of threshold with A) is smallest for medium velocities and larger for lower and higher velocities.

This result does not depend upon the scaling method, but the scaling method makes it easier to define comparable parameter values. For example, without scaling one would have to measure thresholds for a range of pixel sizes and field velocities (deg/sec) and find the parameter combination giving minimum threshold values. The above conclusion would then still hold if the comparison across eccentricities is done for the optimal parameter conditions at each eccentricity. It is obviously "unfair" to just measure motion-detectability as a function of eccentricity for objects of constant size or of constant texture-grain and of constant velocity in terms of deg/sec, since acuity changes strongly with eccentricity. Velocity should be constant in terms of acuity-units per time-unit if a comparison is to be made across eccentricities. The differences in threshold values between the different positions are smallest for the optimal (scaled) velocities of one or two pixels shift between consecutive frames (Figs 6 and 7). The fact that these scaled velocities are optimal irrespective of A and E (Fig. 5) means that our scaling method has the merit of normalizing velocity values quite satisfactorily throughout the visual field. It is hard to discern any pattern in the results at all if the velocities are converted to deg/sec and plotted as such. Our scaling is a simple first order normalization, roughly optimized (van de Grind *et al.*, 1983) for motion detection by the nasal retina, but it serves its purpose of simplifying the presentation and interpretation of the results very well.

Although it would be possible in principle to give a more detailed analysis of the inhomogeneity, for example by statistical methods or with a Fourier series analysis of the periodic threshold-change as a function of A (e.g. Figs 7 and 8), this does not seem sensible for the present data set. The influence of the size of the stimulus on the amplitude of the inhomogeneity is very strong (e.g. Fig. 3) and for threshold values of, say, 25 and higher a relatively small decrease of the stimulus size easily makes the threshold value infinite (no motion seen, even without noise). This instability near threshold means that a more fine-grained analysis of the inhomogeneity requires a different type of experiment. For example, one could measure the threshold stimulus-size as a function of position. Such an extension of the measurement procedure was beyond the scope of the present project.

Anisotropies

Figure 9 presents some of the results for the two main observers on the influence of motion direction (α) on the SNR threshold. The figure allows a comparison of the results at $A = 0°$ (open symbols) to those at $A = 90°$ (solid symbols) for a relatively low and a medium scaled velocity value (0.25 and 1 pixel/frame, respectively), and at the three eccentricities of 6, 24 and 48'.

Figure 9 is illustrative of the main findings regarding the anisotropies, viz. that the thresholds for relatively slow vertical motion near the vertical meridian are very much higher than those for either horizontal motion or for any motion direction at the other positions in the visual field. As will be substantiated below, the (low-velocity) anisotropies are absent at $A = 0$, 45, 180 and 315°, relatively small to medium-sized for the positions (A values) 135 and 225°, respectively, but clearcut at 90 and 270° (the vertical meridian).

The reason why we plotted results for only two positions ($A = 0$ and 90°) in Fig. 9 is that this type of graph easily gets too cluttered to be interpreted. We plotted all results in this form for all the combinations of values for A, E, and V. From this it became clear that some compression of data was necessary and that it would be imperative to develop a criterion for judging the significance of threshold-modulations with α. For example, are the humps in the graphs of the lower row of Fig. 9 significant? Can we call this an indication of some anisotropy? The extreme modulations in the upper graphs are no problem in this respect. It is easily demonstrated to any observer that a stimulus-size exists for moving random-pixel arrays, where he can clearly see horizontal movement at $A = 90°$, but not a vertical movement at otherwise identical stimulus parameters (the same holds at position $A = 270°$). Thus the basic low-velocity anisotropy is very robust and clear-cut and it can be demonstrated at virtually any eccentricity of more than a few degrees.

The method we developed to judge the strength of the anisotropies took the results into account from a thorough visual inspection of many graphs of a type like those in Fig. 9. This initial analysis showed that all potential anisotropies consisted either of a difference between vertical and horizontal motion directions or between radial and tangential directions. At $A = 0$, 90, 180 and 270° vertical and horizontal directions are of course identical to radial and tangential directions, but at the other positions ($A = 45$, 135, 225 and 315°) it was often difficult to decide from inspection whether

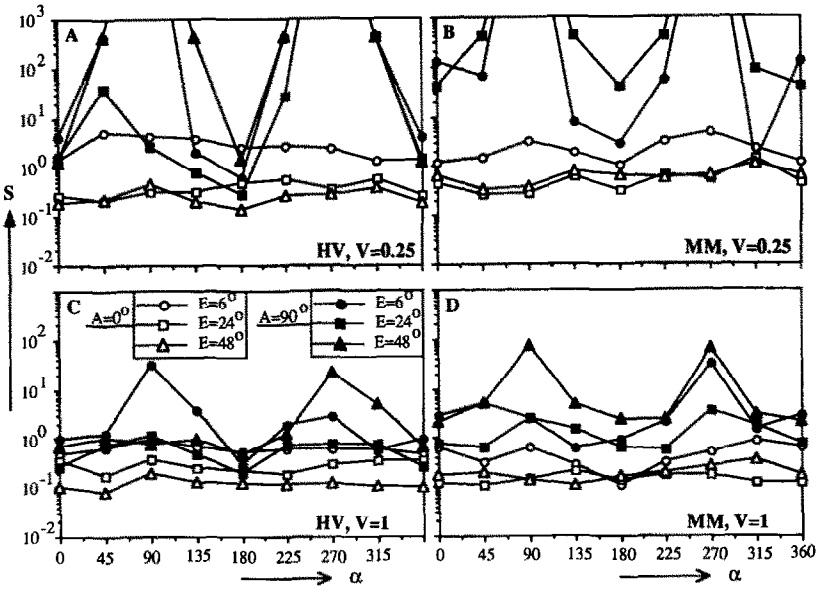

FIGURE 9. Threshold SNR values as a function of motion direction α for a few specific combinations of eccentricity (E) and position (A). The open symbols refer to isotropic positions on the horizontal meridian, namely $A = 0°$ for the eccentricities 6, 24 and 48°. The solid symbols refer to positions on the vertical meridian with strong anisotropies, namely $A = 90°$, eccentricities 6, 24, and 48°. The upper panels are for a "low" velocity, the lower panels for a medium velocity, the left hand panels for observer HV, the right hand panels for MM. Anisotropies, seen as a strong change of S with α, are found for both observers at all three eccentricities for the position $A = 90°$, at least at low velocities. The lower panels illustrate that the anisotropies are small but still noticeable at a medium velocity of $V = 1$ pixel/frame. They disappear at higher velocities (not shown).

potential anisotropies had their main axes in the vertical–horizontal or in the radial–tangential orientation. It was obvious, however, that directions differing by 180° did not usually differ much in threshold. Thus we quantified the potential anisotropies by the following real numbers:

$$Q = \{S(\alpha = 90) + S(\alpha = 270)\}/\{S(\alpha = 0) + S(\alpha = 180)\} \quad (2)$$

$$R = \{S(\alpha = A) + S(\alpha = A + 180)\}/\{S(\alpha = A + 90) + S(\alpha = A + 270)\} \quad (3)$$

where $S(\alpha = x)$ stands for the threshold SNR value for motion direction $\alpha = x$, A is the position in degrees and the constants also have the dimension degrees. To the extent that the threshold octagons approximate to an elliptical shape the quantifiers Q and R of (an)isotropy simply equal the ratio of the length of the main axes. In some of the experiments we measured S for 16 (Fig. 2) or more directions of motion, so it seemed convenient not to take a measure of anisotropy that relied specifically on the number of directions sampled. It would be simple to generalize these measures to the case of non-perpendicular main axes, but in our results the minimum and maximum threshold values were (if they were sufficiently different) virtually always found for perpendicular directions. From the definitions it follows, that $Q = R$ for the positions 90 and 270° and $Q = 1/R$ for the positions 0 and 180°. The differences, if any, between Q and R values are only relevant for the non-horizontal and non-vertical directions.

In order to develop a criterion to judge the strength of the anisotropies we first calculated the numbers Q and R for all values of A for velocities from $V = 0.25$ through $V = 4$ pixels/frame and separately for the eccentricities 6, 24 and 48° and the two main observers. It is first important to get an impression of the statistical distribution of the Q and R values. Therefore we present histograms in Fig. 10 of the Q values calculated for the two main observers. In Fig. 10(A) we included all Q values for both observers (MM and HV) combined for the velocities $V = 0.25$, 0.5, 1, 2 and $V = 4$, and the eccentricities $E = 6$, 24 and 48°. The histogram in Fig. 10(A) is "bimodal", but of course the second mode cannot be illustrated in its entirety, since many Q values of this mode were infinite. If any one of the numerator terms in formula (2) is infinite and the denominator values are both finite Q is infinite. In some cases both numerator and denominator were infinite leading to an indeterminate result (not included in the histograms). The really strong anisotropies occurred at low velocities (see below and Fig. 9) and contributed the infinite values of Q, which were a substantial portion (about half) of the cases reported in Fig. 10(A) as >10.

Figure 10(A) already suggests a form of the distribution of Q values for the isotropic conditions, viz. the left hand mode of the bimodal distribution. From inspection of the threshold octagons (like those in Fig. 4, but blown up in size) we judged the following conditions to be "isotropic" for observer HV: $A = 0, 45, 180, 315°$, all eccentricities. The corresponding Q values are represented in the histogram of Fig. 10(B) and provide us with an estimate of the distribution of Q values for isotropic conditions. This distribution has a mean of 1.7

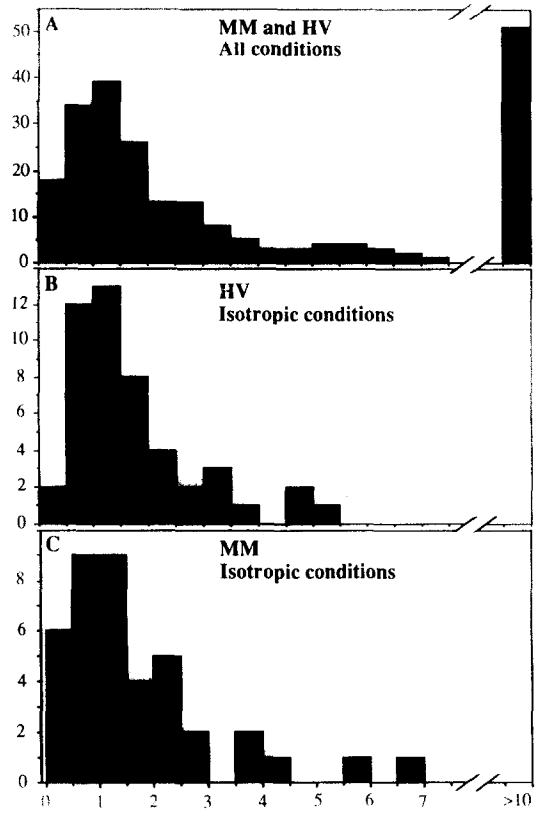

FIGURE 10. Histograms of Q values, where Q is a measure of the strength of an anisotropy oriented along horizontal–vertical axes. Q is defined in formula (2) of the text. The horizontal axes show the categorization of Q values in 16 bins of 0.5, up to $Q = 8$. All Q values ≥ 10 are counted in the bin on the extreme right. About half of the counted "large" Q values were infinite. (A) Shows that the distribution for all Q values for both main observers is bimodal. In (B) and (C) we present histograms of Q values for conditions which looked fairly isotropic in plots such as those of Fig. 4 (see the text for details). On the basis of these three histograms we propose to define "strongly anisotropic" conditions as those for which $Q \geq 10$. For $Q \leq 3$ it seems reasonable to speak of "isotropy", whereas the intermediate region ($3 < Q < 10$) might signify weak to medium anisotropies. This intermediate case is not discussed further in this paper. Obviously for Q below $\frac{1}{3}$ or $\frac{1}{10}$ we should give a similar verdict, but for a long axis of the threshold-ellipse (octagon) in the horizontal rather than vertical direction.

and a variance of 1.3. The same is done for observer MM in Fig. 10(C). However, for this observer we had to leave out the low velocity results at $E = 48'$ ($V = 0.25$ and 0.5). There the anisotropies at $A = 90$ and 270° had such broad peaks that they "spilled over" to $A = 45$ and 180°, leading to anisotropy characteristics at these positions. We think the results in Fig. 10 are reasonably clearcut. One can argue about "significance" in the range of Q values between, say, 3 and 8, but by and large it seems reasonable to define a "strong" anisotropy as one with a Q value in excess of about 8–10. To analyse potential anisotropies in the middle range of Q values (e.g. 3–8) would require a different type of experiment, with many repetitions of the measurements at any given stimulus condition to get a handle on repeatability-statistics. For our purposes it suffices to characterize the most convincing anisotropies, with Q values higher than, say, 10.

Since the anisotropies appeared to be qualitatively independent of eccentricity (for our eccentricities of 6, 24 and 48'), we averaged the Q and R values across eccentricities to get the results of the panels (A–F) in Fig. 11. In (F) we give the results separately for the different eccentricities at one velocity, viz. $V = 1$, the velocity where the maxima are still clearcut but finite (in contradistinction with the results for the lower velocities, where the maxima are always infinite). The results in Fig. 11 are for observer HV, whereas Fig. 12 gives the corresponding results for observer MM.

Applying our criterion for a (strong) anisotropy (Q or R values in excess of 10) we immediately see the anisotropy at $A = 90°$ for the low velocity-range up to and including $V = 1$ pixel/frame. The anisotropy at $A = 270°$ is below our criterion-value for the medium velocity $V = 1$. The solid symbols in these panels are for the Q values and the open symbols for the R values, so we see in Fig. 10(C) that there is a strong radial tangential anisotropy at the position 225°. Looking at the breakdown for the three eccentricities in Fig. 10(F) we see that the three eccentricities are not unanimous in this respect. Only at $E = 48'$ one can speak of a strong anisotropy for the position 225°. It can also be seen in Fig. 11(F), that the results for the different eccentricities agree very well for the positions 90 and 270°, even though these $Q = R$ values do not always reach our criterion value. At $V = 4$ we again see a value above criterion for $A = 225°$, this time representing a horizontal–vertical anisotropy (Q above 10). A look at the results for the three eccentricities separately showed that this anisotropy is present at the lower eccentricities 6 and 24', but not at 48'. Since no analogous results at $A = 225°$ were found for the other observer we regard this finding as idiosyncratic. The low-velocity anisotropies at $A = 90°$ and 270° on the other hand are found for all our (five) observers and therefore represent the main message.

Figure 12 shows that the results for the other main observer (MM) agree quite well with those of HV (Fig. 11). A more detailed study for each of the eccentricities separately showed another peculiar result, again at $A = 225°$, but this time at $V = 2$. Figure 12(F) illustrates this: a Q value of 0.06 was found at $E = 48'$. This means an inverse anisotropy: here the thresholds in the horizontal direction were higther than those in the vertical direction. Suffice it to surmize that position $A = 225°$ appears to be a goldmine of subject-specific idiosyncrasies (see also Fig. 2). Taken together Figs 11 and 12 convey the simple message that strong anisotropies are found for low velocities at the positions along the vertical meridian and that no clear case results for or against the assumption of a radial–tangential rather than horizontal–vertical orientation for the anisotropies at the oblique directions. In most cases (one exception was discussed in relation with Fig. 11 for observer HV and the conditions $A = 225°$, $E = 48'$, $V = 1$) the Q values for the oblique directions are somewhat higher than the R values, showing a slightly stronger tendency for a vertical–horizontal than for a radial–tangential orientation of the anisotropy. The matter can only be resolved further by a more detailed study involving much more

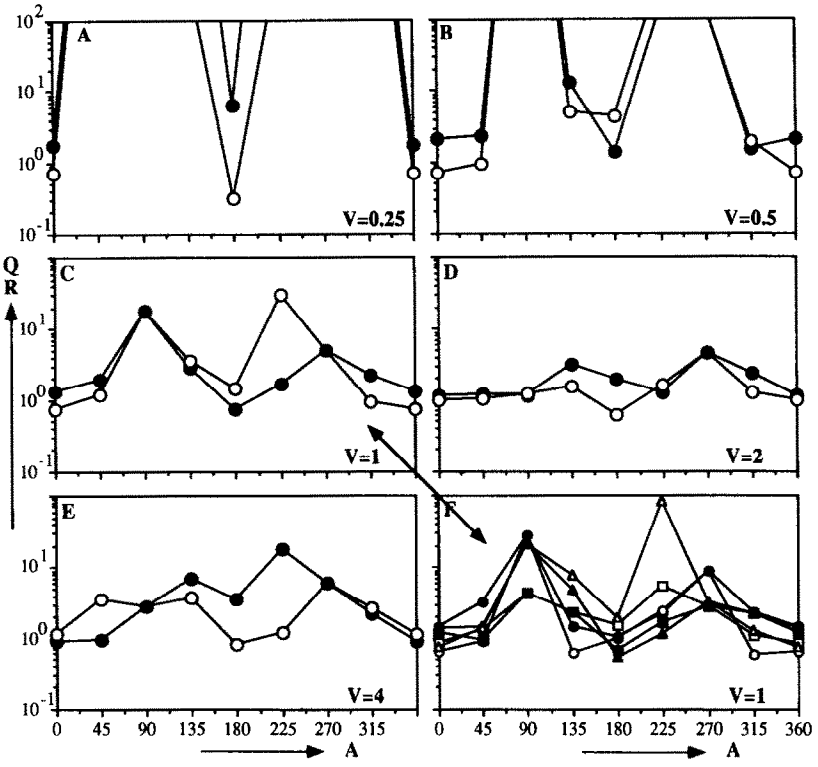

FIGURE 11. Observer HV: average Q or R values as a functon of position A. The Q values [formula (2)] are presented as solid symbols, the R values [formula (3)] as open symbols. Both were averaged across eccentricities for (A–E). The "strong" anisotropies are those for which Q or R or both equal 10 or more (or are smaller than 0.1). This occurs mainly at the lower velocities, up to and including $V = 1$ pixel/frame. If $Q > R$ the anisotropy has a predominantly horizontal–vertical orientation, if $R > Q$ it is more clearly oriented in a radial–tangential fashion (see text). At $A = 90$ and 270° $Q = R$ (by definition) and at $A = 0$ and 180° $Q = 1/R$. The latter "symmetry" in log–log coordinates of Q and R values relative to 1 cannot be seen in this figure due to the separate averaging of Q and R across eccentricities. (A–E) Are for different velocities ($V = 0.25$ through $V = 4$ pixels/frame), whereas (F) gives a breakdown of the graphs of (C) in terms of the constituent graphs for the separate eccentricities. Symbols in (F): circles, $E = 6°$; squares, $E = 24°$; triangles, E = 48°; the solid symbols refer to Q values, the open symbols to R values.

data along the oblique directions. The above results can provide guidelines for the choice of stimulus parameters for such a study.

DISCUSSION

McColgin ▸(1960) studied movement thresholds in peripheral vision for oscillating and rotating line stimuli, which were meant to simulate the situation of detecting in the peripheral visual field motion of the hands of panel meters in an aircraft. He used 48 eccentric positions ($E = 20$, 40, 60 and 80°, combined with A values incremented in steps of 30° from 0 to 360°) and constructed threshold isograms. The resulting isograms were elliptical with the long axis oriented along the horizontal meridian of the visual field. In our experiments we only used 24 peripheral positions (but of course we used a whole range of velocities and looked at anisotropies), which is not enough to draw meaningful (SNR) threshold isograms. Nevertheless, our results are qualitatively similar to those of McColgin. For example, the global form of the graphs in Fig. 7 can be viewed as resulting from the intersection of equi-eccentricity circles with elliptical threshold isograms, provided the isogram ellipses extend a bit further in the visual field of the nasal retina, than into that of the temporal retina (thresholds at $A = 180°$ are consistently higher than those at $A = 0°$ for the same eccentricity).

More recently Scobey and van Kan (1991) did a perimetric study of displacement sensitivity for a small (22 × 22′ or for eccentricities below 5 deg 5′ × 5′) white luminous target, 1 log unit above the local luminance threshold drifting in 10 msec at a constant velocity from a start position to its end position for the trial. This means that the velocity covaried with the displacement distance. They presented isometric curves of displacement threshold in the visual field (their Fig. 3) and studied the directional anisotropies at each position. The isometric curves were egg-shaped, with the long axis on the horizontal meridian and a longer extension into the nasal retinal field than into the temporal retinal field. This is again analogous to our findings for the detection of coherent motion in noise degraded random pixel arrays. In some respects the analysis of anisotropies for displacement detection by Scobey and van Kan (1991) appears to give somewhat different results from the findings described in this paper. However, the differences might be smaller than they appear at first sight. Scobey and van Kan found a stronger tendency for a tangential–radial orientation of the anisotropy, where we find mixed results, sometimes more horizontal–vertical and sometimes more radial–tangential in orientation. However,

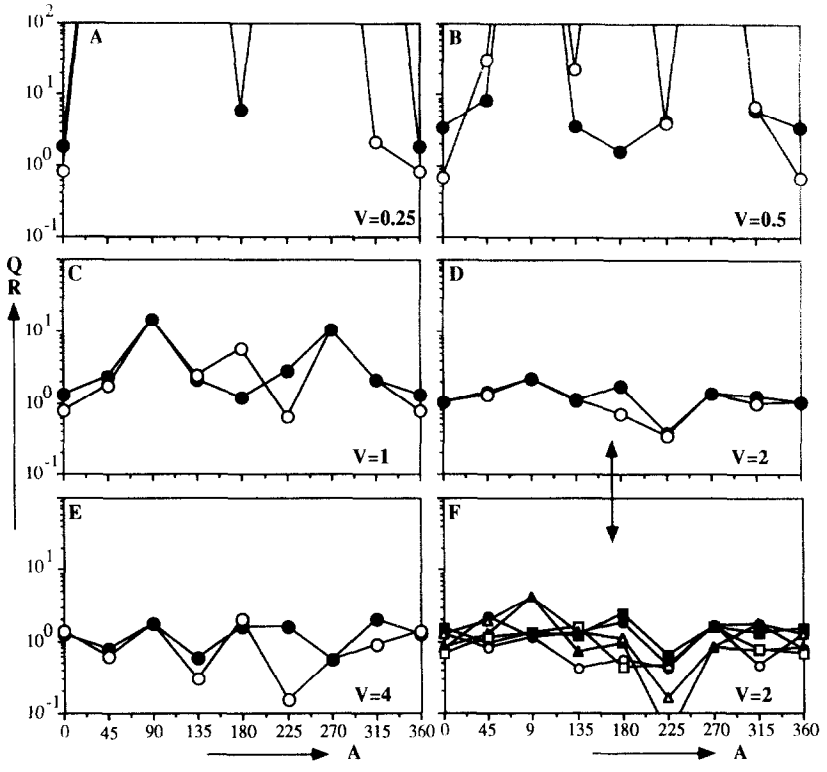

FIGURE 12. Observer MM. The format of this figure is the same as of Fig. 11, except that (F) now gives a breakdown of the averaged results of (D), as indicated by the correspondence arrow. Symbols in (F): circles, $E = 6$; squares, $E = 24$; triangles, $E = 48$; the solid symbols refer to Q values, the open symbols to R values. Also in the other panels open symbols refer to R, solid symbols to Q values.

neither their nor our data allow a very strong conclusion in this respect. The results agree for the vertical and horizontal meridians. It should be kept in mind that the two experiments might tap different mechanisms, but the similarities are intriguing. Our Q and R values might seem high compared to the ratio's of long to short axes of the threshold ellipses of Scobey and van Kan, but this might be due to the amplification effect of the SNR method. For their displacement thresholds the range of values is very restricted, whereas our SNR thresholds map the subject's judgments onto a range of values from, say, 0.04 to infinity. Given these methodological differences we think the agreements in the results are more impressive than the differences.

The analogy of the results of McColgin for "long-range" motion stimuli, our results for "short-range" motion stimuli and the results of Scobey and van Kan for displacement detection (as in noticing displacement of the clock's hour hand over time) suggests that the inhomogeneity is part of a common front-end system. We don't think the explanation can be found in optical factors, since our method is very robust against defocusing. Random pixel arrays contain a wide band of spatial frequencies (white spectrum), and blurring merely decreases the power in the highest available frequencies a bit. As long as there is sufficient bandwidth and signal power to activate about equally many retinal receptive fields as under optimal optical correction the SNR threshold is not influenced very strongly by defocus. We have often verified this informally by adding inappropriate supplementary lenses to defocus the retinal image a few diopters. Thus neither the reported inhomogeneities nor the anisotropies are likely due to optical factors such as spherical defocus or off-axis astigmatism. The inhomogeneity might very well start at the retinal level, however. Primates, such as humans, have a weak form of a visual streak. The density of retinal ganglion cells is greater on the nasal part of the horizontal meridian than at the same eccentricity on the temporal part of the horizontal meridian, but the density is lower still at the same eccentricity on the vertical meridian (Stone & Johnson, 1981). Assuming that the detection of coherent motion is a cooperative process (van Doorn & Koenderink, 1982b, 1983; van Doorn *et al.*, 1984; van de Grind *et al.*, 1986) more cells covered by the stimulus means a lower SNR threshold. This threshold would be expected to improve in inverse proportion to the square-root of the number of stimulated bilocal detectors. Thus the findings of a lower threshold SNR value on the horizontal meridian as compared to the vertical meridian qualitatively fits the known inhomogeneous distribution of retinal ganglion cells.

Can one similarly point at a possible anatomical substrate for the anisotropies? The anatomical findings of elongated dendritic trees in monkey (Schall, Perry & Leventhal, 1986) and man (Rodieck, Binmoeller & Dineen, 1985) would qualitatively go in the right direction to explain the anisotropies. Since these fields are elongated in the radial direction, the resolution should be better in the tangential direction. This would be especially important for low velocities, which are detected by bilocal detectors with the smallest subfields

(van de Grind *et al.*, 1986). Since the fields are smaller in the tangential direction there would (for an isotropic coverage factor) also be more of them per unit of retinal tangential distance covered by the stimulus than per unit distance in the radial direction. This could mean a stronger summation and recruitment effect (van de Grind *et al.*, 1983) in the tangential direction than for motion in the radial direction. Our findings might also correlate with the anisotropies of cortical mapping. The cortical mapping of the horizontal meridian in the macaque monkey appears to be isotropic, whereas the map is stretched along the cortical representation of the vertical meridian (along the V1–V2 border) by about 2 to 1 (Van Essen, Newsome & Maunsel, 1984; for a review see LeVay & Nelson, 1991). It would probably be premature and presumptious to attempt to make too much out of these analogies between our psychophysical results and the structural mappings. A detailed linking hypothesis would require a quantitative model of the structure and function of motion detectors and the process of their cooperation and competition. At least one can conclude that the anatomical findings do not point in the wrong direction.

Another possible approach to the question of linking structure and function in the case of the presented anisotropies and inhomogeneities is as follows. The anisotropies were found to be strong only in the low velocity range, whereas inhomogeneities are both noticeable at low and at high velocities, but not at medium velocities. In terms of the idea of separate P-B, P-I, and M streams (e.g. Livingstone & Hubel, 1988) one might surmise that the anisotropies are properties of the P-I stream (form and low velocities), and that the inhomogeneities are common to or present in both the M (high velocities) and the P-I streams. It would at least be interesting to see whether the apparent corollary of this suggestion, that the anisotropies should be absent in area MT, but that MT should show the reported inhomogeneities, can withstand further scrutiny. It would also be interesting to see whether the same type of anisotropies and inhomogeneities can be found for long-range motion stimuli. This would support the thesis that both long-range and short-range motion stimuli are analysed by the same front-end motion analysis system (Cavanagh & Mather, 1989; Bischof & Di Lollo, 1990; van de Grind *et al.*, 1992). The similarity between the results of McColgin (long-range motion stimuli) and of this study (short-range stimuli) regarding the inhomogeneity of the monocular visual field for motion processing is suggestive in this respect.

We have shown that a simple scaling of stimulus dimensions according to formula (1) equates the optimal velocity at all positions tested to about 1–2 pixels/frame. This simplifies the results quite a bit. The finding that thresholds along the vertical meridian at the studied eccentricities are higher than at corresponding eccentricities on the horizontal meridian, whereas the threshold must be the same where the meridians cross, suggests that a meridian-specific scaling would homogenize the visual field for motion detection. We think this would be helpful to some extent if it is restricted to the idea of making circles out of ellipses for iso-threshold lines. However, our results also show that one should not be too ambitious in this respect. The low thresholds at $E = 24^{\circ}$ for $A = 135$ and 180° shown in Fig. 4 illustrate that a simple two-dimensional scaling regime would not eliminate all differences. It seems unattractive to develop still more complex scaling formulae, with both A, E and possibly even V as parameters. A complete and perfect subject-specific scaling regime would simply be a mirror image of the anisotropies and inhomogeneities of the subject in question, and thus be useless as a simplification metric.

Our scaling method purports to be based on the principle of equalizing velocity throughout the visual field in terms of the number of acuity-units (number of activated receptive fields) per time unit or, perhaps better still, per receptive field sampling-time unit. If this is a valid idea, one should expect a high similarity between anisotropies or inhomogeneities measured in acuity tests and those reported in this paper for the detection of coherent motion. (If acuity relates to the number of cells per unit area in the retina and the SNR threshold depends upon the number of stimulated cells one would expect a similar relation to anatomy, even though our SNR values do not depend very strongly on eye optics, whereas acuity is not robust against defocus.) Judging from a recent review by Fiorentini and Berardi (1991) this expectation is more or less borne out. Resolution is higher for grating patterns oriented radially than tangentially (Rovamo, Virsu & Hyvarinen, 1982). This is analogous to most of our data, except those obtained on the horizontal meridians, where we found isotropy for coherent motion detection, whereas Rovamo *et al.* (1982) report anisotropy for grating-acuity. Also the findings by Pointer and Hess (1989), who report orientational anisotropies in the peripheral visual field along the vertical meridian have a certain similarity to our results. The best correspondence between our data and those on acuity is no doubt the global difference between the nasal and temporal half fields. Visual acuity is higher in the temporal than in the nasal visual field of both monkeys and humans and this correlates with differences in cell densities (Curcio, Sloan, Packer, Hendrickson & Kalina, 1987; Curcio & Allen, 1990; Curcio & Sloan, 1992; Fiorentini & Berardi, 1984, 1991; Marzi & Di Stefano, 1981; Merigan & Katz, 1988; Rovamo & Virsu, 1979; Wässle, Grünert, Röhrenbeck & Boycott, 1989). An analogous naso–temporal asymmetry is also obvious in our results (e.g. compare the right half of Fig. 4 to the left half or compare results for mirror-image positions such as $A = 45$ and 135° in Figs 5–8). Since some of the details might depend upon the methods used or idiosyncrasies of the subjects, we feel that a more detailed comparison is not sensible and that the best way to explore the similarities further would be a complete perimetry for acuity and coherent motion detection in one and the same subject. This would be a heavy task.

Moreover, stimulus size, contrast, adaptation level, stimulus pattern, and many more parameters would have to be manipulated as well. Unfortunately few vision scientists (the authors included) have the endurance, patience and craving for empirical data necessary to compile such a coherent body of reference data.

REFERENCES

Ball, K. & Sekuler, R. (1980). Human vision favors centrifugal motion. *Perception, 9*, 317–325.

Bischof, W. F. & Di Lollo, V. (1990). Perception of directional sampled motion in relation to displacement and spatial frequency: Evidence for a unitary motion system. *Vision Research, 30*, 1341–1362.

Braddick, O. (1974). A short-range process in apparent motion. *Vision Research, 14*, 519–527.

Cavanagh, P. & Mather, G. (1989). Motion: The long and short of it. *Spatial Vision, 4*, 103–129.

Chang, J. J. & Julesz, J. (1983). Displacement limits, directional anisotropy and direction versus form discrimination in random-dot cinematograms. *Vision Research, 23*, 639–646.

Curcio, C. A. & Allen, K. A. (1990). Topography of ganglion cells in human retina. *Journal of Comparative Neurology, 300*, 5–25.

Curcio, C. A. & Sloan, K. R. (1992). Packing geometry of human cone photoreceptors: Variation with eccentricity and evidence for local anisotropy. *Vision Neuroscience, 9*, 169–180.

Curcio, C. A., Sloan, K. R., Packer, O., Hendrickson, A. E. & Kalina, R. E. (1987). Distribution of cones in human and monkey retina: Individual variability and radial asymmetry. *Science, 236*, 579–582.

van Doorn, A. J. & Koenderink, J. J. (1982a). Temporal properties of the visual detectability of moving spatial white noise. *Experimental Brain Research, 45*, 179–188.

van Doorn, A. J. & Koenderink, J. J. (1982b). Spatial properties of the visual detectability of moving spatial white noise. *Experimental Brain Research, 45*, 189–195.

van Doorn, A. J. & Koenderink, J. J. (1983). The structure of the human motion detection system. *IEEE Transactions, SMC-13*, 916–922.

van Doorn, A. J. & Koenderink, J. J. (1984). Spatiotemporal integration in the detection of coherent motion. *Vision Research, 24*, 47–53.

van Doorn, A. J., Koenderink, J. J. & van de Grind, W. A. (1984). Limits in spatio-temporal correlation and the perception of visual movement. In van Doorn, A. J., van de Grind, W. A. & Koenderink, J. J. (Eds), *Limits In Perception* (pp. 203–234). Utrecht: VNU Science Press.

van Doorn, A. J., Koenderink, J. J. & van de Grind, W. A. (1985). Perception of movement and correlation in stroboscopically presented noise patterns. *Perception, 14*, 209–224.

Fiorentini, A. & Berardi, N. (1984). Right-hemisphere superiority in the discrimination of spatial phase. *Perception, 13*, 695–708.

Fiorentini, A. & Berardi, N. (1991). Limits in pattern discrimination: Central and peripheral factors. In Kulikowski, J. J., Walsh, V. & Murray, I. J. (Eds), *Vision and visual dysfunction* (Vol. 5, Chap. 20, pp. 266–276). New York: Macmillan.

Fredericksen, R. E., Verstraten, F. & van de Grind, W. A. (1993). Spatio-temporal characteristics of human motion perception. *Vision Research*. In press.

Georgeson, M. A. & Harris, M. G. (1978). Apparent foveofugal drift of counterphase gratings. *Perception, 7*, 527–536.

van de Grind, W. A., van Doorn, A. J. & Koenderink, J. J. (1983). Detection of coherent movement in peripherally viewed random-dot patterns. *Journal of the Optical Society of America, 73*, 1674–1683.

van de Grind, W. A., Koenderink, J. J. & van Doorn, A. J. (1986). The distribution of human motion detection properties in the monocular visual field. *Vision Research, 26*, 797–810.

van de Grind, W. A., Koenderink, J. J. & van Doorn, A. J. (1987). Influence of contrast on foveal and peripheral detection of coherent motion in moving random-dot patterns. *Journal of the Optical Society of America, A, 4*, 1643–1652.

van de Grind, W. A., Koenderink, J. J. & van Doorn, A. J. (1988). Distance invariance in human global movement detection. *Perception, 17*, 350, A12.

van de Grind, W. A., Koenderink, J. J. & van Doorn, A. J. (1992). Viewing-distance invariance of movement detection. *Experimental Brain Research, 91*, 135–150.

van de Grind, W. A., Koenderink, J. J., van Doorn, A. J., Milders, M. V. & Voerman, H. (1990). Inhomogeneities and anisotropies of the visual field for motion detection. *Investigative Ophthalmology and Visual Science, 31*, 1179.

Koenderink, J. J. (1986). Optic flow. *Vision Research, 26*, 161–180.

Koenderink, J. J., van Doorn, A. J. & van de Grind, W. A. (1985). Spatial and temporal parameters of motion detection in the peripheral visual field. *Journal of the Optical Society of America A, 2*, 252–259.

LeVay, S. & Nelson, S. B. (1991). Columnar organization of the visual cortex. In Leventhal, A. G. (Eds) *The neural basis of visual function. Vision and visual dysfunction* (Vol. 4, Chap. 11, pp. 266–315). New York: Macmillan.

Livingstone, M. & Hubel, D. (1988). Segregation of form, color, movement, and depth: Anatomy, physiology and perception. *Science, 240*, 740–749.

Marzi, C. & Di Stefano, M. R. (1981). Hemiretinal differences in visual perception. *Documenta Ophthalmologica Proceedings Series, 30*, 273–278.

Mateeff, S. & Hohnsbein, J. (1988). Perceptual latencies are shorter for motion towards the fovea than for motion away. *Vision Research, 28*, 711–719.

Mateeff, S., Bohdanecky, Z., Hohnsbein, J., Ehrenstein, W. H. & Yakimoff, N. (1991a). A constant latency difference determines directional anisotropy in visual motion perception. *Vision Research, 31*, 2235–2237.

Mateeff, S., Yakimoff, N., Hohnsbein, J., Ehrenstein, W. H., Bohdanecky, Z. & Radil, T. (1991b). Selective directional sensitivity in visual motion perception. *Vision Research, 31*, 131–138.

McColgin, F. H. (1960). Movement thresholds in peripheral vision. *Journal of the Optical Society of America, 50*, 774–779.

Merigan, W. H. & Katz, L. M. (1988). Visual acuity across the macaque retina. *Neuroscience Abstracts*, 1120.

Moulden, B., Kingdom, F. & Gatley, L. F. (1990). The standard deviation of luminance as a metric for contrast in random-dot images. *Perception, 19*, 79–101.

Nakayama, K. (1984). Biological image processing: A review. *Vision Research, 25*, 625–660.

Pointer, J. S. & Hess, R. F. (1989). The contrast sensitivity gradient across the human visual field: With emphasis on the low spatial frequency range. *Vision Research, 29*, 1133–1151.

Reichardt, W. (1961). Autocorrelation, a principle for the evaluation of sensory information by the central nervous system. In Rosenblith (Ed.), *Sensory communication* (pp. 303–317). Cambridge, Mass.: MIT Press.

Rodieck, R. W., Binmoeller, K. F. & Dineen, J. (1985). Parasol and midget ganglion cells of the human retina. *Journal of Comparative Neurology, 223*, 115–132.

Rovamo, J. & Virsu, V. (1979). An estimation and application of the human cortical magnification factor. *Experimental Brain Research, 37*, 495–510.

Rovamo, J., Virsu, V. & Hyvarinen, L. (1982). Resolution of gratings oriented along and across meridians in peripheral vision. *Investigative Ophthalmology and Visual Science, 23*, 665–670.

van Santen, J. P. H. & Sperling, G. (1984). Temporal covariance model of human motion perception. *Journal of the Optical Society of America A, 1*, 451–473.

van Santen, J. P. H. & Sperling, G. (1985). Elaborated Reichardt detectors. *Journal of the Optical Society of America A, 2*, 300–321.

Schall, J. D., Perry, V. H. & Leventhal, A. G. (1986). Retinal ganglion cell dendritic fields in old-world monkeys are oriented radially. *Brain Research, 368*, 18–23.

Scobey, R. P. & van Kan, P. L. E. (1991). A horizontal stripe of displacement sensitivity in the human visual field. *Vision Research, 31*, 99–109.

Stone, J. & Johnson, E. (1981). The topography of primate retina: A study of the human, bushbaby and new- and old-world monkeys. *Journal of Comparative Neurology, 196*, 205–223.

Van Essen, D. C., Newsome, W. T. & Maunsell, J. H. R. (1984). The visual field representation in striate cortex of the macaque monkey: Asymmetries, anisotropies, and individual variability. *Vision Research, 24*, 429–448.

Wässle, H., Grünert, U., Röhrenbeck, J. & Boycott, B. B. (1989). Cortical magnification factor and the ganglion cell density of the primate retina. *Nature, 341*, 643–646.

Acknowledgements—This work was supported by the US Air Force Office of Scientific Research, Grant No. 87-0380. We are grateful to M. Lankheet, and R. E. Fredericksen for their critical reading of the manuscript and their many useful comments.